Trans Indian Inst Met (2024) 77(3):607–614
https://doi.org/10.1007/s12666-023-03148-0

ORIGINAL ARTICLE

Influence of Mechanical Attrition on Protective Properties of Anomalous Electrodeposited Ni-Co Alloys

Kaveh Hajizadeh[1] · **Vahid Abbasi Chianeh**[1]

Received: 15 May 2023 / Accepted: 9 October 2023 / Published online: 3 November 2023

Abstract Ni-Co alloys with different compositions were electrodeposited from additive-free Watt's type electrolytes utilizing mechanical-assisted electrodeposition. SEM, XRD, microhardness, and potentiodynamic polarization tests were used to investigate the effects of mechanical attrition speed and electrolyte composition on electrodeposits. Increased attrition speed resulted in reduced Co content in films with fcc crystal structure and raised Co content in hcp crystal structures. The microhardness values raised significantly, while the corrosion resistance was reduced by applying mechanical attrition. In order to choose the best electrodeposit, the *C* factor—a ratio of hardness to corrosion current density—is introduced. Based on the *C* factor, the deposits with 4 at% (Co/Co + Ni) in electrolyte and attrition speed of 600 rpm were selected as the best condition, which resulted in an alloy with a smooth and reflective surface containing 32 at% (Co/Co + Ni) with a hardness of 480 HV and corrosion current density close to that of pure nickel electrodeposits.

Keywords Mechanically assisted electrodeposition · Anomalous co-deposition · Ni-Co alloys · Corrosion resistance · Microstructure

1 Introduction

Electrodeposition is well-known as a viable and economical technique for producing dense alloys and coatings with excellent properties, e.g., high strength, hardness, magnetic properties, thermal stability, corrosion, and wear resistance [1–6]. Organic additives play an important role in traditional plating processes, such as improved properties due to reduced grain growth rate in nickel electrodeposited films by sodium lauryl sulfate, saccharin, and 2-butyne-1,4-diol as additives [7–11]. However, these additives adversely affect some of the properties, such as magnetic and anti-corrosion properties, due to the segregation of sulfur and carbon into grain boundaries [12–14]. Several mechanical and physical techniques, including rotating electrode technology, laser plating, jet plating, mechanical attrition or controlled abrasion, ultrasonic wave-assisted plating, and other ways, have been used to overcome the limits of organic additives. [15–21]. Mechanical attrition-assisted plating (MAP) has been widely investigated, which improves the deposition rate and the quality of electrodeposited films. Mechanical disturbance of electrolytes containing hard particles such as SiC, SiO_2, Al_2O_3, glass balls, or soft nonconductive particles results in abraded cathode surfaces, which possess smooth surfaces, refined grains, increased hardness, and excellent corrosion resistance [16–18, 22–25].

In addition to the use of magnetic recording tapes, composite coatings, photo-thermal conversion devices, rocket technology, and astronautics, Ni-Co films are extensively used in protective and decorative plating applications. The ability of nickel and cobalt to alloy in all ratios enables the potential uses of their properties to be explored in a wide range of conditions [26, 27]. Moreover, the surface treatment business and the microelectronics sector, which uses electrodeposition for microfabrication, have shown significant interest in the electrodeposition of Ni-Co alloys [26, 28, 29].

Whether from simple or complex baths, Ni-Co alloys electrodeposit anomalously. For the iron group binary alloys, this phenomenon has received an extensive review, and

✉ Vahid Abbasi Chianeh
v.abbasi@uut.ac.ir

[1] Department of Materials Engineering, Urmia University of Technology, P. O. Box 57155-419, Urmia, Iran

numerous models have been created to predict this behavior [30–34]. Anomalous co-deposition is characterized by preferential deposition of the less noble metal from baths containing different metallic Ions. The mechanism of anomalous co-deposition is not fully understood, despite the numerous models that have been proposed. The formation of the less noble metal's hydroxide precipitate at the cathode due to a local pH increase is one of the theories for anomalous co-deposition [35–39]. However, anomalous co-deposition has not been studied sufficiently in physical or mechanically assisted electrodeposition techniques. Considering the different suggested mechanisms for anomalous co-deposition, it seems that the MAP method would enhance the anomalous co-deposition of Ni-Co alloys while attaining the mentioned benefits of utilizing MAP.

The aim of this research is to utilize the MAP method for electroplating Ni-Co films from a sulfate bath containing Ni and Co ions without additives and study the effect of mechanical attrition on the corrosion and structural properties of anomalous co-deposited films.

2 Experimental Details

As substrates, mild steel plates were placed within the electrodeposition chamber. Steel substrate and nickel plate anode dimensions were 100*10*2 mm^3 and 10*10*2 mm^3, respectively. The substrates were degreased in a one molar NaOH solution at 40 °C for 1 min and then rinsed with distilled water. Degreased substrates were activated in a 20 wt% HCl solution at room temperature for 1 min, and then they were completely cleaned with distilled water right away before placing in the electrodeposition chamber. The Ni-Co alloy coatings were electrodeposited in a modified Watt's bath that contained varying concentrations of cobalt. 250 g/L of $NiSO_4.6H_2O$, 0–50 g/L of $CoSO_4.7H_2O$, 40 g/L of $NiCl_2.6H_2O$, and 40 g/L of H_3BO_3 were all present in the electroplating bath. Electrodeposition was carried out in a 1000-mL glass beaker filled with 550 g of glass balls with a diameter of 1mm and 250 ml of electrolyte. Mechanical rotation was applied with a blade of 50*100*2 mm^3. For each sample, electrodeposition was carried out for 20 min at a current density of 0.02 A/cm^2, while the bead rotation speed was set to 0, 300, or 600 rpm. Figure 1 shows the schematics of utilized equipment. The deposition bath's temperature was held constant at 50 ± 1 °C, while H_2SO_4 and NaOH were used to adjust the pH to 4.3 ± 0.1.

The crystalline structures of electrodeposited alloys were examined by X-ray diffractometry (XRD, Simens D 5000) using Cu Kα radiation operated at 40 kV/30mA. A field emission scanning electron microscope (MIRA III TESCAN) with an energy-dispersive spectroscopy system was used to investigate the deposits' surface appearance, chemical composition, and microstructure. Vickers microhardness tests were performed utilizing an MDPEL-M400 microhardness tester under 50 g load force and 10 s indentation time. The average of seven measurements was used to get the microhardness values. Investigation on the corrosion resistance of Ni-Co alloy coatings was conducted using the Ivium vertex instrument for potentiodynamic polarization measurements. All electrochemical experiments were conducted in the 3.5 wt% NaCl solution at room temperature without stirring. The reference electrode was a saturated calomel electrode (SCE), and the counter electrode was a platinum electrode with an exposed surface approximately ten times larger than the working electrode. The samples were cleaned in ethanol and rinsed with distilled water before potentiodynamic polarization tests were conducted. The open circuit potential (Eocp) was obtained by submerging the cleaned samples in the corrosive liquid for almost 60 min. Following this, the potentiodynamic sweep was conducted with a rate of 1 mV/s across a potential range of −300 to + 300 mV concerning Eocp.

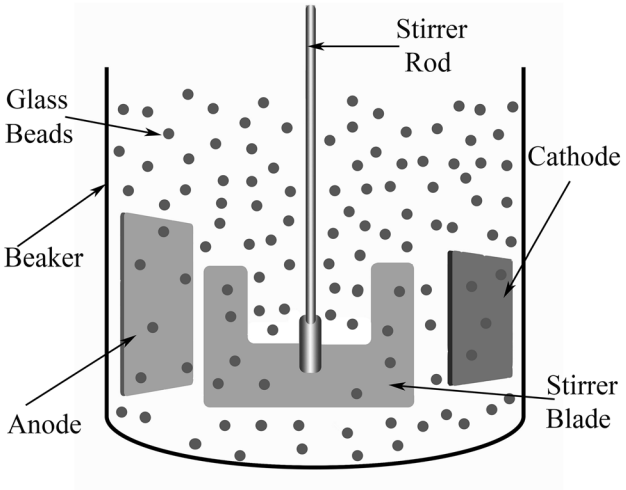

Fig. 1 Schematics of utilized equipment for mechanical attrition-assisted electrodeposition

3 Results and Discussion

The cobalt content of electrodeposited films was examined using energy-dispersive spectroscopy (EDS). Figure 2 illustrates the cobalt contents of the electrodeposited films as a function of the electrolytes Co concentration. Different rotation speeds of 300 and 600 rpm were used to electrodeposit samples in every electrolyte composition through mechanical attrition. As a reference sample for comparison,

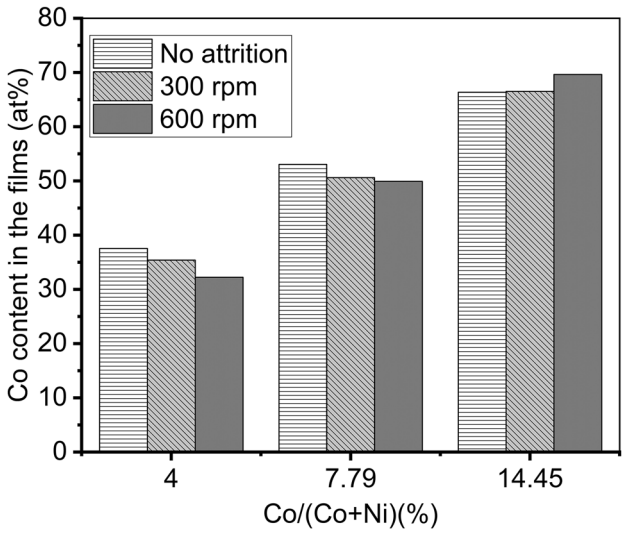

Fig. 2 Co content of electrodeposited films by different mechanical attrition speeds of 0, 300, and 600 rpm against the Co concentration of the electrolyte

one sample was electrodeposited in each electrolyte without mechanical attrition.

As shown in Fig. 2, the cobalt content in the electrodeposited films increases as the cobalt concentration of the electrolyte rises. Furthermore, cobalt contents in all electrodeposited films are significantly higher than the corresponding cobalt amount in the electrolyte. The preferential electrodeposition of cobalt indicates that co-deposition of Ni-Co alloys occurs in an anomalous manner. Several mechanisms for the anomalous co-deposition of Ni-Co alloys have been suggested. According to a report by Qiao et al., raising the Co concentration in the electrolyte causes an increase in the amount of Co in the electrodeposited layer because it increases the Co content of the diffusion layer in the electrolyte, which is consistent with the findings of this study [20]. However, according to this mechanism, electrolyte rotation results in decreased diffusion layer thickness; thus, more Co content in the electrodeposited layers should be achieved.

In contrast, in this research, it is detected that increasing the rotation speed of the bead bed results in decreased Co content in the films except for the samples that were electrodeposited in electrolytes with high Co ions concentration (14.45%). Other mechanisms include absorption of metal hydroxides at the cathode, which results in increased Co content of the film, and the suppression of nickel deposition by deposition of Co ions [38, 39]. These two mechanisms could explain why the Co content in the film decreases by increasing the rotation speed of the bead bed. Mechanical scratching of the cathode surface could result in less metal hydroxide adsorption and thus could result in less cobalt concentration in the films. Moreover, the mechanical force

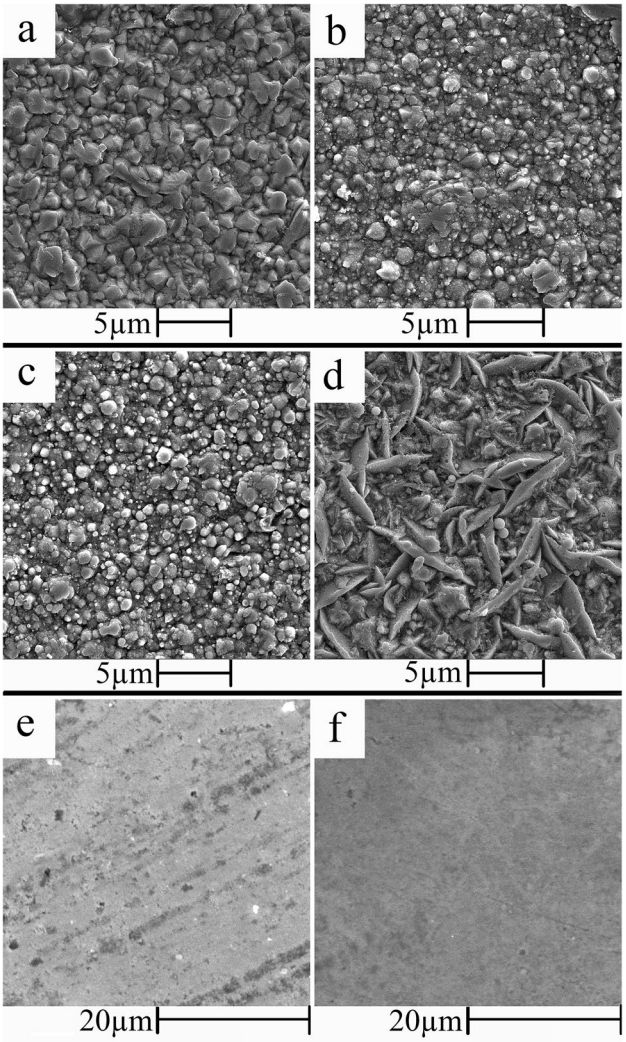

Fig. 3 SEM images of electrodeposited films with different Co concentrations in electrolyte and attrition speed of **a** pure nickel and 0 rpm, **b** 4% Co concentration and 0 rpm, **c** 7.79% Co concentration and 0 rpm, **d** 14.45% Co concentration and 0 rpm, **e** 7.79% Co concentration and 300rpm, **f** 7.79% Co concentration and 600 rpm

from the high-speed rotation of the bead bed could activate the electrodeposited Co on the cathode and reduce the Ni electrodeposition suppression mechanism. However, it seems that more investigation has to be done to clarify the more dominant mechanism.

The surface morphology of electrodeposited Ni-Co alloys was investigated using SEM, as shown in Fig. 3. It could be seen that increasing the Co content in the films has resulted in decreased colony size. The rising of the Co content from 0 to 54 at% changes the polygonal crystallite morphology (Fig. 3a) to globular (Fig. 3c). Further rising of the Co content to 66 at% changes the crystallite morphology to acicular (Fig. 3d). The dominant morphology of the sample with 66 at% Co is a regular branched structure that includes acicular

crystallites with a length of 2–6 µm. Electrodeposition in stirred ball bed results in a smooth surface that indicates the effect of the mechanical strike of the balls on the surface while electrodepositing the alloys. Figure 3e and f shows the surface of the samples electrodeposited from 40 g/l Co electrolyte with the rotation speed of 300 and 600 rpm, respectively. It could be seen that increasing the rotation speed results in a smoother and more reflective surface than samples deposited without balls in the electrolyte.

Figure 4 shows XRD patterns of electrodeposited samples with different Co contents and rotation speeds of the ball bed. Considering Fig. 4, it could be seen that increasing the Co content in the electrodeposited alloys results in changing the crystal structure from fcc to hcp. According to Fig. 2, it could be seen that in samples with a Co content of 70% at, the crystal structure is hcp, while at Co contents lower than 50% at, the dominant structure is fcc which has been reported in other research [40]. Moreover, it could be seen that mechanical attrition results in peak broadening and changing the ratio of peak intensity. Peak broadening indicates the grain refinement and microstrains in the structure that could be due to mechanical attrition. However, mechanical attrition results in the formation of (111) texture in the fcc structure and (002) texture in the hcp structure. Texture

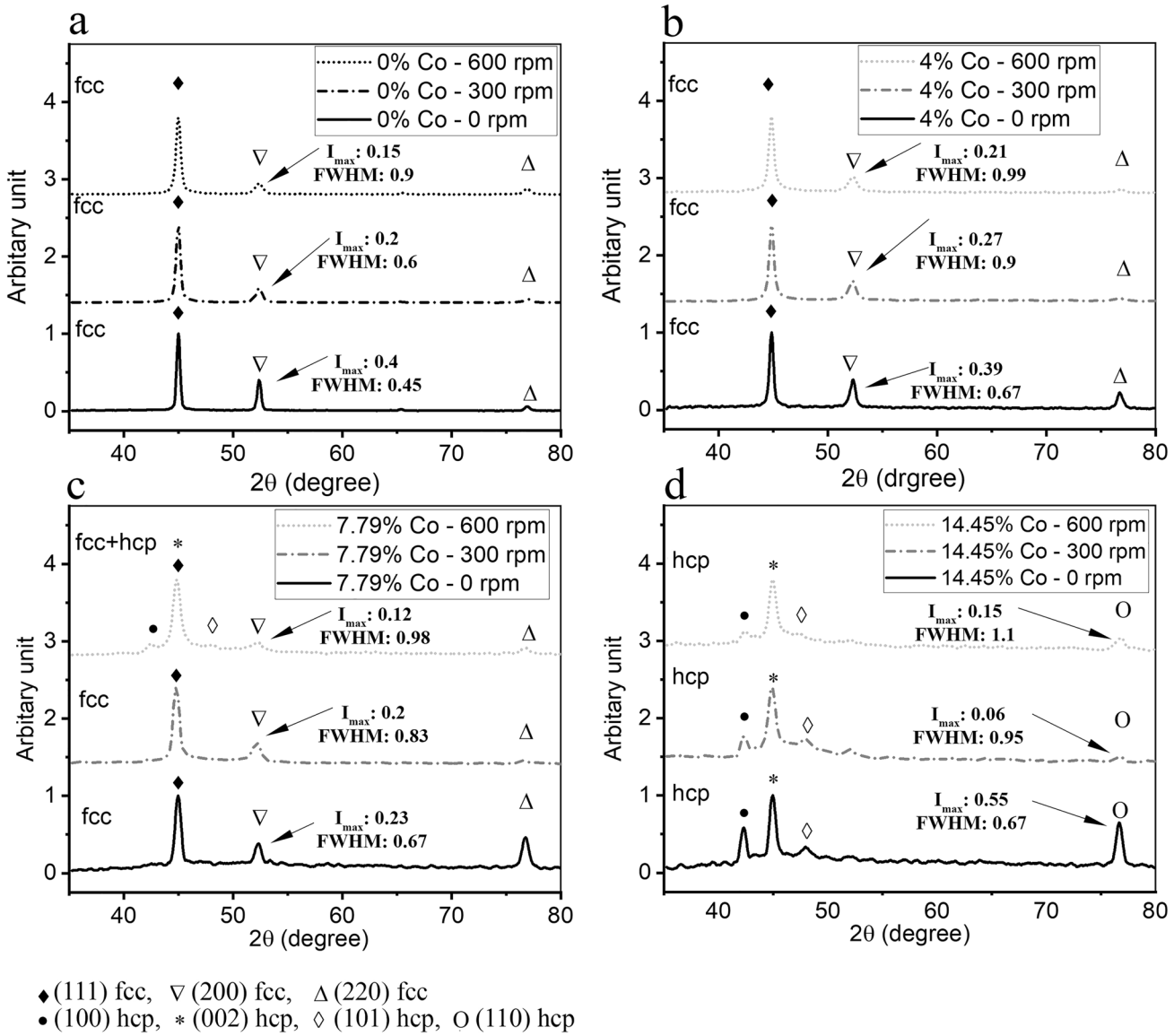

Fig. 4 XRD pattern of electrodeposited films in electrolytes with Co concentration of 0, 4, 7, 79, and 14.45% and attrition speed of 0, 300, and 600 rpm

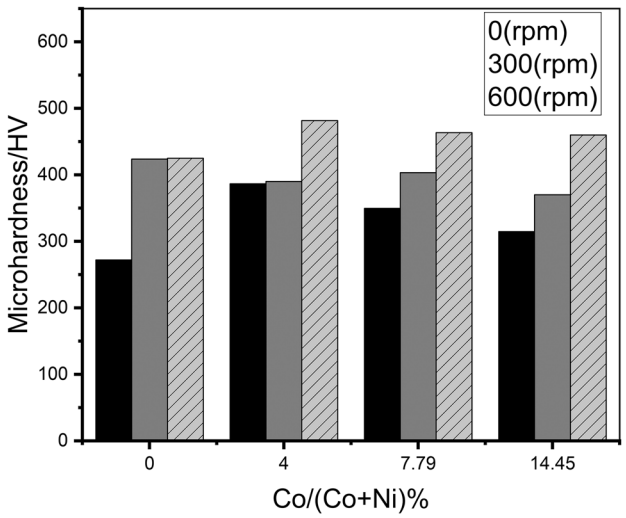

Fig. 5 Microhardness value of electrodeposited films against Co concentration of electrolyte for attrition speeds of 0, 300, and 600 rpm

formation and also grain refinement could affect the mechanical and physical properties. The effects of compositional and microstructural changes on the mechanical and corrosion properties of the samples were examined using microhardness and polarization tests.

Results of the microhardness test are plotted in Fig. 5 against Co content and mechanical attrition speed. According to Fig. 5, it could be seen that mechanical attrition with the rotation speed of 300 rpm resulted in an increase in the microhardness value from 270 to 420 HV in pure Ni films, while increasing the rotation speed to 600 rpm did not have a significant effect on hardness. The increased hardness could be due to grain refinement obtained because of decreased growth speed and increased appropriate nucleation sites while electroplating. Moreover, for samples electrodeposited from Ni-Co electrolyte with 4% Co content, it could be seen that a rotation speed of 300 rpm did not significantly affect the hardness while increasing the rotation speed resulted in increased hardness. This dissimilar behavior could be due to different microhardness values of electrodeposited samples without mechanical attrition but with varying amounts of Co content. Increased hardness due to Co addition could be the reason for the resistance of the electrodeposited films against refinement by low-speed mechanical attrition. Increasing the Co content of the electrolyte to 7.79% and up to 14.45% results in decreased microhardness value compared to 4% Co content. At the same time, mechanical attrition could continually affect the hardness by increasing the attrition speed so that both speeds of 300 and 600 rpm have improved the hardness significantly.

Figure 6 displays potentiodynamic polarization curves. By applying the Tafel method, the curves were used to extrapolate the corrosion potentials and current densities, which are tabulated in Table 1. Considering the corrosion current densities, it could be seen that the corrosion current density rises as the Co concentration in the bath increases up to 7.79%, whereas a Co content of 14.45 results in a drop, which may be caused by the crystal phase changing to hexagonal. Pure Ni has a nobler corrosion potential, but its corrosion current density is the lowest. The corrosion resistance of electrodeposited films in baths with different Co concentrations is not influenced similarly by electrodeposition under agitated beads. Electrolyte with 0 and 4% (Co/Co + Ni) concentration results in electrodeposits which show the same trend in corrosion current density across ball bed stirring speed. The current density increases by applying 300 rpm, but increasing the speed to 600 rpm results in decreased current density. But when using an electrolyte with 7.79% Co concentration, the corrosion current density decreases to 19. 05 and 14.12 μA/cm^2 when stirring with a ball bed at speeds of 300 and 600 rpm, respectively. Additionally, when an electrolyte with 14. 45% concentration of cobalt is used, the resulting electrodeposits have an hcp crystal structure. Changing the stirring bed speed to 300 and 600 rpm leads to a decrease in corrosion current density to 10. 71 μA/cm^2 and an increase to 20. 41 μA/cm^2, respectively. Such a behavior could be due to microstructural changes that has occurred by mechanical forces applied by ball bed stirring. Microstructural changes have been discussed in XRD and SEM results. The smooth surface of samples discovered by SEM due to mechanical attrition as well as the elimination of (200) and (220) crystal plane peaks as a texture change sign is the recorded evidence for affected microstructures by mechanical attrition during electrodeposition. These effects are in addition to grain refinement and increased density of crystal defects that could be inferred from peak broadening in XRD test results. Moreover, mechanical attrition changes the composition of co-electrodeposited alloys.

However, in addition to microhardness and XRD tests, corrosion test findings indicate that the mechanically enhanced electrodeposition procedure needs to be optimized for an improved outcome. In the case of pure Ni, the rotation speed of 300 and 600 rpm result in the same increased hardness value of 420 HV compared to conventional electrodeposited film with a hardness value of 280 HV. At the same time, the corrosion current density of samples deposited under the varied speed stirring ball bed has a meaningful difference from each other. Still, the film prepared under 600 rpm differs slightly from the

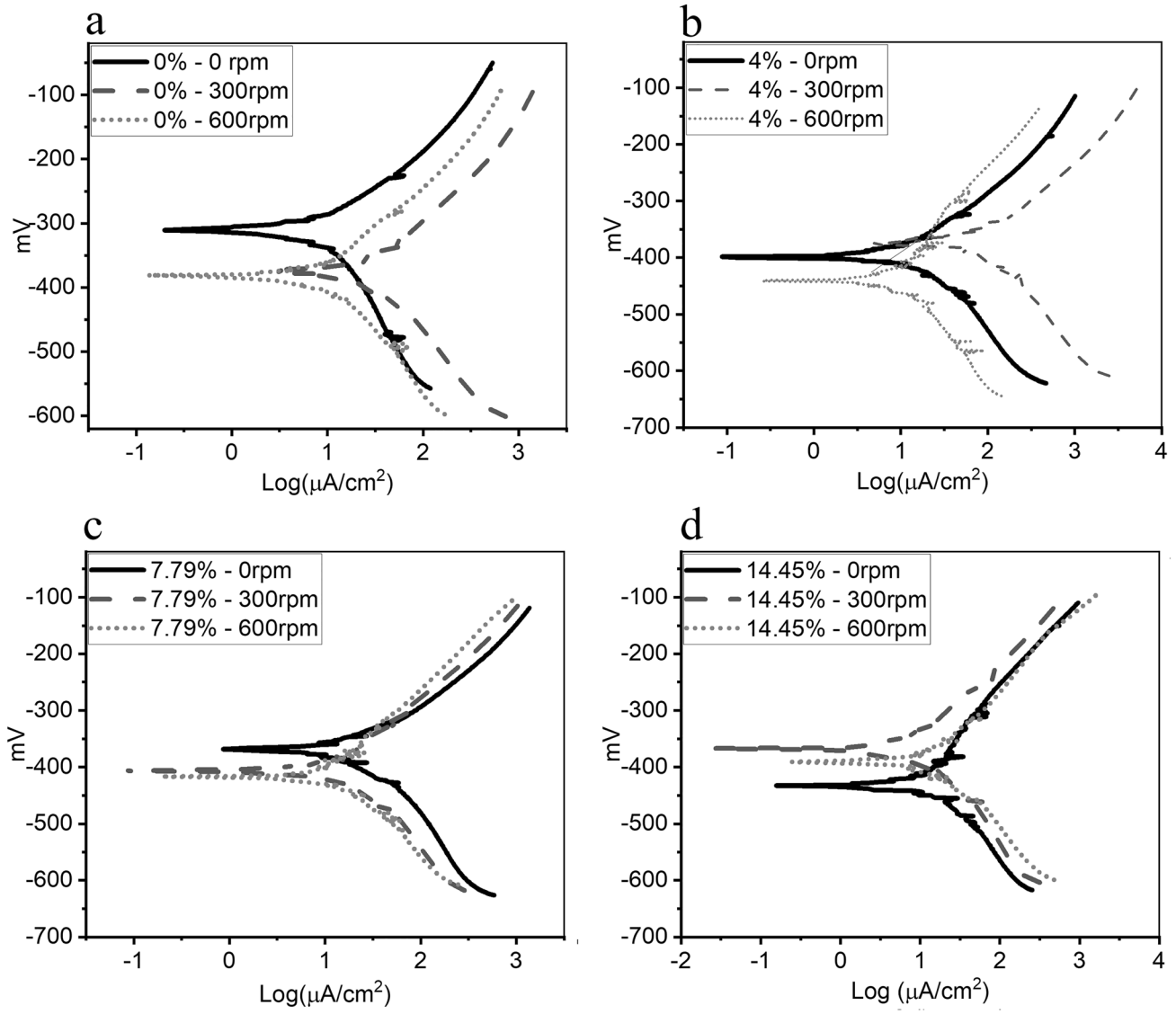

Fig. 6 Potentiodynamic polarization curves of the samples in 3.5% NaCl solution at room temperature

conventionally electrodeposited film in corrosion current density. Therefore, each alloy obtained from the electrodeposition of a distinct electrolyte with different attrition speeds has different hardness or corrosion resistance. Because of the various effects of attrition speed on the mechanical and corrosion current density, a parameter is introduced as *C* that refers to the hardness of the sample divided by corrosion current density. The *C* factors are listed in Table 2 for the samples prepared from different electrolytes and various speeds of attrition. According to *C* factors tabulated in Table 2, it could be concluded that the best properties are obtained with a high-speed attrition of 600 and the bath containing 4% of Co concentration, and the worst properties are obtained from the same bath but with an attrition speed of 300 rpm. This result indicates that mechanical attrition could change the alloy properties drastically, so it's a priority to introduce a process that applies homogenous mechanical attrition on all fragments of the deposited films.

The above discussions indicate that the corrosion behavior of electrodeposited Ni-Co alloy results from the simultaneous effect of different parameters. The higher hardness/

Table 1 Corrosion potentials, current densities and polarization resistance of electrodeposited films extrapolated from curves in Fig. 6 by applying the Tafel method

Co (%)	Stirring Speed (rpm)	R_p (KΩ/cm^2)	$J_{cor.}$ (μA/cm^2)	$E_{Cor.}$ (mv)
0	0	3.9	8.7	−300
	300	0.54	28.2	−369
	600	3.35	9.33	−376
4	0	1.63	15.85	−387
	300	0.256	89.12	−366
	600	1.08	9.77	−431
7.79	0	1.132	32.35	−363
	0	2.055	19.05	−392
	0	0.937	14.12	−392
14.45	0	1.684	15.13	−418
	300	2.420	10.71	−350
	600	2.091	20.41	−386

Jcor ratio can be correlated to (i) moderate grain size or crystal defect density, (ii) obtained phase/crystal structure, (iii) relative majority of the preferred orientation (texture) of a distinct crystal plane, (IV) chemical composition, and (V) surface morphology. However, to determine the most crucial factor affecting the *C* factor of electrodeposited alloys under mechanical attrition, more detailed studies are necessary to determine the effect of each parameter on the hardness/corrosion rate ratio.

4 Conclusion

Chemical composition, surface morphology, crystal structure, hardness, and corrosion resistance of electrodeposited Ni-Co alloys with different Co contents of electrolyte were examined under different mechanical attrition speeds. Results indicate that MAP could obviously enhance the hardness and corrosion resistance of different alloy compositions. Hardness to corrosion current density has been introduced as a *C* factor to determine the optimum electrodeposition condition for obtaining an alloy with high hardness and corrosion resistance. The results show that the superposition of different structural parameters and compositions generates alloys with very different *C* factors of 4.4 to 49.3 HV/Jcor. The highest *C* factor is obtained from a bath containing 4% Co with an attrition speed of 600 rpm. The minor *C* factor is also obtained from the bath containing 4% of Co but at the rotation speed of 300 rpm. However, applying mechanical attrition in all electrolytes has resulted in increased hardness value. Corrosion of samples obtained under mechanical attrition indicates that each electrolyte with a different amount of Co content has a different response to applying various speeds of mechanical attrition. These results suggest that mechanical attrition should be used under distinct conditions for the best *C* factor. The *C* factor changes drastically with changing the mechanical attrition speed because mechanical attrition impacts very different structural parameters that could affect the electrochemical and mechanical properties.

Table 2 The *C* factor obtained from dividing hardness values of electrodeposited films by corrosion current densities in Table 1

Attrition speed	0	300	600	0	300	600	0	300	600	0	300	600
%Co	0	0	0	4	4	4	7.79	7.79	7.79	14.45	14.45	14.45
C factor (HV/J_{Cor})	31.3	15	45.5	24.4	4.4	49.3	10.8	21.17	32.8	20.8	34.5	22.5

Declarations

Conflict of interest The authors declare that they have no known competing financial interests or personal relationships that could have appeared to influence the work reported in this paper.

References

1. Karimzadeh A, Aliofkhazraei M, and Walsh F C, *Surf Coat Technol* **372** (2019) 463. https://doi.org/10.1016/j.surfcoat.2019.04.079
2. Mishra R, and Balasubramaniam R, *Corros Sci* **46** (2004) 3019. https://doi.org/10.1016/j.corsci.2004.04.007
3. Godon A, Creus J, Cohendoz S, Conforto E, and Savall C, *Scr Mater* **62** (2010) 403. https://doi.org/10.1016/j.scriptamat.2009.11.038
4. Ebrahimi F, Bourne G R, Kelly M S, and Matthews T E, *Nanostructured Mater* **11** (1999) 343. https://doi.org/10.1016/S0965-9773(99)00050-1
5. Dalla Torre F, Swygenhoven H V, and Victoria M, *Acta Mater* **50** (2002) 3957. https://doi.org/10.1016/S1359-6454(02)00198-2
6. Wasekar N P, Haridoss P, Seshadri S K, and Sundararajan G, *Wear* **296** (2012) 536. https://doi.org/10.1016/j.wear.2012.08.003
7. Rashidi A, and Amadeh A, *Surf Coat Technol* **204** (2009) 353. https://doi.org/10.1016/j.surfcoat.2009.07.036
8. Pavlatou E A, Raptakis M, and Spyrellis N, *Surf Coat Technol* **201** (2007) 4571. https://doi.org/10.1016/j.surfcoat.2006.09.113
9. El-Sherik A, and Erb U, *J Mater Sci* **30** (1995) 5743. https://doi.org/10.1007/BF00356715
10. Das P, Samantaray B, Dolai S, Seshu K S, and Gollapudi S, *Metall Mater Trans A* **52** (2021) 1913. https://doi.org/10.1007/s11661-021-06202-y
11. Lokhande A C, and Bagi J S, *Surf Coat Technol* **258** (2014) 225. https://doi.org/10.1016/j.surfcoat.2014.09.023
12. Wang Y, Cheng S, Wei Q M, Ma E, and Hamza A, *Scr Mater* **51** (2004) 1023. https://doi.org/10.1016/j.scriptamat.2004.08.015
13. Zhang X, Fujita T, Pan D, Yu J S, and Chen M W, *Mater Sci Eng A* **527** (2010) 2297. https://doi.org/10.1016/j.msea.2009.12.005
14. Hu Y, Deb S, Li D, and Huang Q, *Electrochim Acta* **368** (2021) 137594. https://doi.org/10.1016/j.electacta.2020.137594
15. Wu B, Xu B, Zhang B, and Dong S, *Surf Coat Technol* **201** (2007) 5758. https://doi.org/10.1016/j.surfcoat.2006.10.013
16. Lv B, Hu Z, Wang X, and Xu B, *Surf Coat Technol* **270** (2015) 123. https://doi.org/10.1016/j.surfcoat.2015.03.012
17. Ping Z, Ping Z, He Y, Gu C, and Zhang T, *Surf Coat Technol* **202** (2008) 6023. https://doi.org/10.1016/j.surfcoat.2008.06.183
18. Ping Z, He Y, Gu C, and Zhang T, *J Appl Electrochem* **39** (2009) 6879. https://doi.org/10.1007/s10800-008-9734-9
19. Idris J, Christian C, and Gaius E, *J Nanomater* **2013** (2013) 12. https://doi.org/10.1155/2013/841260
20. Qiao G, Jing T, Wang N, Gao Y, and Wang W, *Electrochim Acta* **51** (2005) 85. https://doi.org/10.1016/j.electacta.2005.03.050
21. Liu C, Su F, and Liang J, *Surf Coat Technol* **292** (2016) 37. https://doi.org/10.1016/j.surfcoat.2016.03.027
22. He Y, Fu H F, Li X G, and Gao W, *Scr Mater* **58** (2008) 504. https://doi.org/10.1016/j.scriptamat.2007.10.051
23. Eisner S, *Trans IMF* **51** (1973) 13. https://doi.org/10.1080/00202967.1973.11870257
24. Ning Z, He Y, and Gao W, *Surf Coat Technol* **202** (2008) 2139. https://doi.org/10.1016/j.surfcoat.2007.08.062
25. Zhaoxia P, YUAN J, HE Y, and LI X, *Acta Metall Sin Engl Lett* **22** (2009) 225. https://doi.org/10.1016/S1006-7191(08)60093-9
26. Oriňáková R, Turoňová A, Kladeková D, Gálová M, and Smith R M, *J Appl Electrochem* **36** (2006) 957. https://doi.org/10.1007/s10800-006-9162-7
27. Brenner A, *Electrodeposition of Alloys: Practical and specific information,* Vol 2, Elsevier (1963), ISBN: 978–1–4831–9807–1
28. Li Y, Shan L, Sui Y, Qi J, and Liu J, *J Mater Sci: Mater Electron* **30** (2019) 13360. https://doi.org/10.1007/s10854-019-01703-4
29. Zhang H, Lv Y, Wu X, Guo J, and Jia D, *Chem Eng J* **431** (2022) 133233. https://doi.org/10.1016/j.cej.2021.133233
30. Matlosz M, *J Electrochem Soc* **140** (1993) 2272. https://doi.org/10.1149/1.2220807
31. Zech N, Podlaha E, and Landolt D, *J Electrochem Soc* **146** (1999) 2886. https://doi.org/10.1149/1.1392024
32. Grande W C, and Talbot J B, *J Electrochem Soc* **140** (1993) 675. https://doi.org/10.1149/1.2056141
33. Chen Y, Yang H, Feng H, Yang P, and Shu B, *Today Commun* **35** (2023) 106058. https://doi.org/10.1016/j.mtcomm.2023.106058
34. You Y H, Gu C D, Wang X L, and Tu J P, *Surf Coat Technol* **206** (2012) 3632. https://doi.org/10.1016/j.surfcoat.2012.03.001
35. Bakhit B, and Akbari A, *J Coat Technol Res* **10** (2013) 285. https://doi.org/10.1007/s11998-012-9437-3
36. Hu C, and Bai A, *J Electrochem Soc* **149** (2002) 615. https://doi.org/10.1149/1.1511753
37. Golodnitsky D, Gudin N, and Volyanuk G, *J Electrochem Soc* **147** (2000) 4156. https://doi.org/10.1149/1.1394034
38. Bai A, and Hu C, *Electrochim Acta* **47** (2002) 3447. https://doi.org/10.1016/S0013-4686(02)00281-5
39. Go´ mez E, Ramirez J, and Valle´s E, *J Appl Electrochem* **28** (1998) 71. https://doi.org/10.1023/A:1003201919054
40. Liu P, Chen D, Wang Q, Xu P, Long M, and Duan H, *J Phys Chem Solids* **137** (2020) 1. https://doi.org/10.1016/j.jpcs.2019.109194